Anomalies in the electronic structure of Bi_2Se_3

Deepnarayan Biswas and Kalobaran Maiti
Department of Condensed Matter Physics and Materials' Science,
Tata Institute of Fundamental Research, Homi Bhabha Road, Colaba, Mumbai - 400 005, India.
(Dated: February 13, 2015)

We studied the electronic structure Bi_2Se_3 employing density functional theory. The calculations show that the Dirac states primarily consists of the states at the interface of surface and sub-surface quintuple layers and the emergence of the Dirac states depends on the surface terminations in sharp contrast to their surface character expected for such systems. This manifests the complexity of real materials and the realization of topological order in real materials as an outstanding problem. We discover that the surface character of the Dirac states can be achieved by adsorption of oxygen on Bi-terminated surface due to the change in covalency by the relatively more electronegative oxygens.

PACS numbers: 73.20.At, 03.65.Vf, 68.43.-h

Topological insulators are characterized by metallic states at the surface of bulk insulators protected by time reversal symmetry and strong spin-orbit coupling [1, 2]. Due to time reversal symmetry protection, the electrons moving on the surface cannot be scattered in the reverse direction without spin flip. Thus, the corresponding energy bands exhibit linear dispersion forming a Dirac cone, which is one of the key signatures in the electronic structure of a topological insulator. Due to such unique electronic properties, these materials are potential candidates for realization of exotic physics such as Majorana Fermions, magnetic monopoles [3, 4]. These materials are also expected to bring immense technological advances and new possibilities in the fields of spintronics, quantum computation, dissipation less charge transfer etc. [2]. While all these realizations require experimental finding of protected topologically ordered surface states on insulating bulk materials, experiments show contrasting scenarios often with instability of topological order. The bulk of almost all the materials studied exhibit metallic phase [5]. Thus, finding of a true topological insulator remains to be an outstanding puzzle.

Engineering new materials for such behavior requires critical understanding of the electronic structure of the materials exhibiting topological order. For example, one of the most studied materials for such behavior is Bi_2Se_3 that shows Dirac cone with its apex at finite binding energy instead of its chemical potential. In addition, several bulk bands are observed at the Fermi level suggesting its metallic bulk electronic structure. Carrier doping due to aging/impurities often inhibits achieving topological transport regime. Some theories predicted relaxation of van der Waals bond as a reason for such behavior [6], while other studies show necessity of unusually large change in bond length to produce the experimentally observed scenario [7]. The surface band bending induced by adsorption of residual gases [8–11], commonly observed in semiconductors, may also give rise to such effect. Interestingly, both positive and negative charge doping due to impurity adsorption have been observed in angle resolved photoemission measurements [11–13]. While all these studies indicate instability of the surface states with aging, impurity adsorption etc., there are studies reporting stable surface behavior [14–16]. Evidently, the behavior of the surface states of these materials is highly anomalous. In order to reveal microscopic details underlying such electronic properties, we calculated the electronic band structure for both surface and bulk employing density functional theory, and discover interesting results, significantly different from the expected behavior of this system.

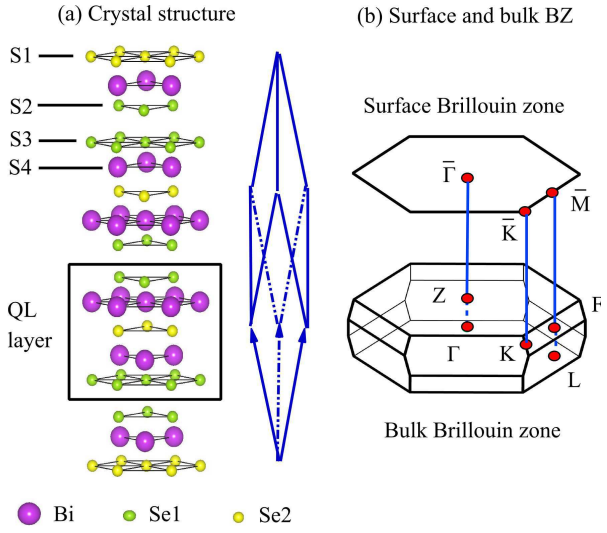

FIG. 1. (a) Crystal structure of Bi_2Se_3 exhibiting atomic arrangement and the rhombohedral unit cell. S1, S2, S3 and S4 denote the layers where the surface terminations are considered in this work. (b) The surface and bulk Brillouin zone (BZ) along with different high symmetry points.

The electronic band structure calculation of Bi_2Se_3 was carried out using full potential linearized augmented plane wave method within the local density approximations [17]. The bulk electronic structure is calculated using the lattice constants, $a = b = 4.18$ Å, $c = 28.7$ Å, $\alpha = \beta = 90^o$ and $\gamma = 120^o$ obtained from the literature

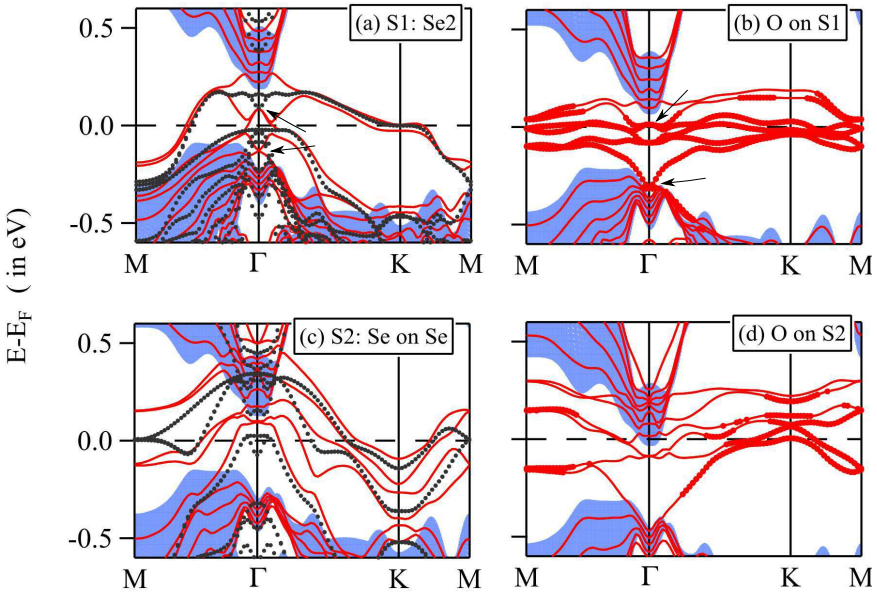

FIG. 2. Band structure of (a) clean and (b) 1 monolayer (ML) O covered S1 terminated surfaces, and (c) clean and (d) 1 ML O covered S2 terminated surface. The black dots show the bands with no spin-orbit coupling and lines are with spin-orbit coupling. The blue region is the projected bulk bands and the red dots denote the bands with more than 50% O contribution.

[18]. In order to investigate the surface electronic structure, we considered the lattice in a 'slab' configuration with at least 5 quintuple layers within the unit cell - the total number of layers varies for different surface terminations. Calculations were carried out for all the possible surface terminations as defined in Fig. 1.

Bi_2Se_3 forms in rhombohedral structure with space group, $R\bar{3}m$. In Fig. 1(a), we show the crystal structure[19] with both hexagonal and rhombohedral axes. It has a layered structure containing quintuple layers consisting of Se1-Bi-Se2-Bi-Se1 layers, where two nonequivalent Se layers are denoted by Se1 and Se2. The quintuple layers are believed to be connected through weak Van der Waals bond [6, 7]; the inter-layer bonding within the quintuple layer is relatively stronger. This indicates a well defined cleavage plane exposing Se1 terminated surface. Recent experiments, however, show signature of both Bi and Se terminated surfaces on cleaving [11, 20] exhibiting significantly different behavior. Thus, we considered the surface terminations S1, S2, S3 and S4 (see figure) representing Se2, Se1 (one Se1 on top of the quintuple layer), Se1 (normal cleavage plane) and Bi terminations, respectively. Fig. 1(b) shows the bulk and surface Brillouin zones with different high symmetry k points. For (111) surface of Bi_2Se_3, the time reversal invariant momenta (TRIM) are the high symmetry points, Γ and M. In addition to the pristine cases, we deposited a monolayer of oxygen on top of the surfaces. The exchange correlation potential is included under generalized gradient approximation (GGA) [21]. Spin-orbit interaction is included as a second order perturbation for Bi and Se atoms [22]. The energy convergence was achieved using $10 \times 10 \times 1$ k-mesh.

The calculations for the bulk Bi_2Se_3 converge to insulating ground state with a band gap of about 0.3 eV consistent with the experimental findings [23–25]. The results from the slab calculations exhibit interesting scenario with very different surface bands near the Fermi level, ϵ_F for different terminations. All the energy bands obtained from slab calculations are doubly degenerate as a symmetric slab geometry has been used [26] for these calculations. In Figs. 2(a) and 2(c), we show the band structure obtained for S1 and S2 cases. The black dots represent the bands without spin-orbit coupling (SOC) and the solid red lines correspond to the calculations including SOC. The shaded area represents the projected bulk bands (PBB) for the SOC case, where the difference in Fermi level between the surface and bulk calculations are compensated by matching the bulk bands away from the Fermi level. The bands appearing in the gap of the PBB are the surface bands. It is evident from the data that SOC leads to a splitting of the spin degenerate bands obtained without SOC [22]. For both the surface terminations, the surface bands cross the Fermi level between surface projected TRIMs, Γ-M odd number of times implying that the material belong to a strong topological insulator class [2]. The bands near ϵ_F consist primarily

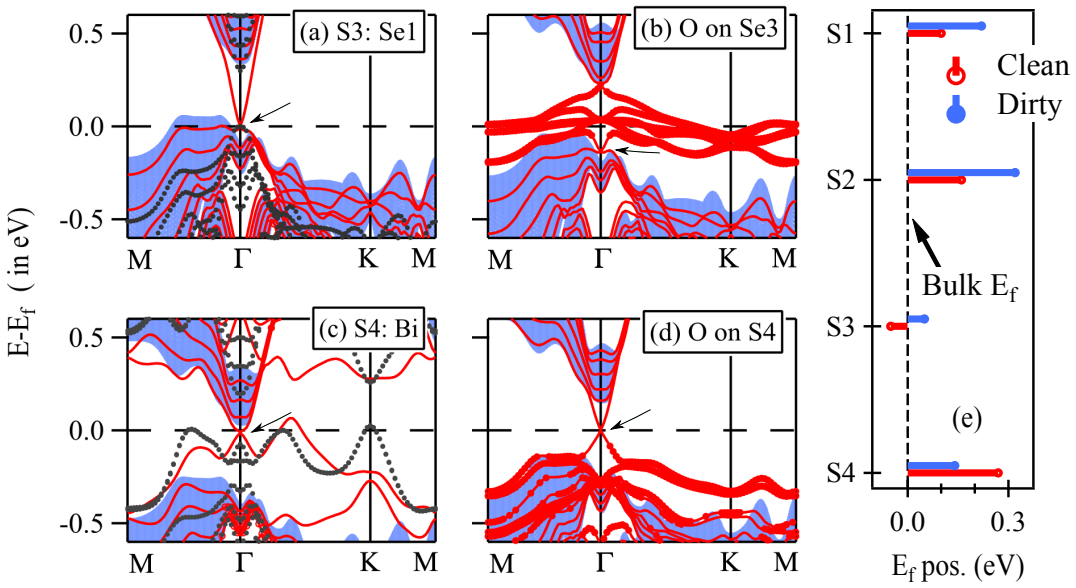

FIG. 3. Energy band structure for (a) S3-terminated, (b) 1 ML oxygen on S3 surface, (c) S4 terminated surface and (d) 1 ML oxygen on S4 surface. (e) Shift of slab Fermi level w.r.t. bulk Fermi level (dotted line) binding energy.

of Se 4p and Bi 6p characters.

For clean Se2 terminated surface, the conduction band maxima and the valence band minima at Γ point shown by arrows in Fig. 2(a) exhibit a separation of about 0.3 eV due to Bi p and Se2 p hybridizations. The band crossing at around -0.16 eV exhibits a scenario akin to a Dirac cone representing topological order. Here, the finite energy of the Dirac point (apex of the cone) is intrinsic to the electronic structure. Impurities/defects play important role in the electronic structure leading to charge carrier doping and introducing local character of the charge carrier [27, 28]. We have verified this in the present case by calculating electronic structure with one monolayer oxygen on the surface. The Dirac point shifts away from ϵ_F as shown by an arrow in Fig. 2(b). An additional pair of bands appear near ϵ_F possessing primarily O 2p character. This is shown by big circles representing more than 50% O 2p contributions in Fig. 2(b). The energy bands near ϵ_F becomes narrower compared to the pristine case suggesting enhancement of local character of the electronic states. The overall shift of the energy bands towards higher binding energies (= negative of the energy shown in the figures) in the later case represents an effective electron doping as expected due to relatively higher electronegativity of oxygen. The results for S2 termination are shown in Fig. 2(c) and 2(d). The energy bands exhibit significantly different behavior with no signature of Dirac cone. Oxygen in this case leads to a band narrowing (see Fig. 2(d)) and effective electron doping as found in the case of S1 termination. However, the oxygen 2p character appears stronger around high symmetry points other than Γ.

The energy bands corresponding to S3 and S4 terminated surfaces are shown in Fig. 3. The results obtained without SOC exhibit finite gap between the valence and conduction bands. Inclusion of SOC leads to the formation of distinct Dirac cone like feature at Γ point at ϵ_F as shown by arrow in the figure. In these terminations, the presence of spin-orbit coupling leads to the surface bands crossing the Fermi level odd number of times between TRIMs, Γ and M providing again the signature of a strong topological insulating phase in these cases [20, 25]. The Dirac point (DP) appears very close to the top of the valence band for Se terminated surface (S3 case) and near bottom of the conduction band on Bi-terminated surface (S4 case).

The most interesting phenomena occurs on deposition of oxygen on these surfaces; the Dirac cone shifts to higher binding energy (∼ 0.14 eV) along with significant narrowing of the energy bands near ϵ_F (see Fig. 3(b)). O 2p-derived additional narrow bands appear in the vicinity of the Fermi level as found in the case of Se2 terminated surface. Fig. 3(d) exhibits the energy bands corresponding to a monolayer oxygen on Bi-terminated surface. The DP shifts away from the bottom of the conduction band and the Dirac cone becomes prominent, better defined with larger slope. Here, the oxygen 2p-derived bands with smaller dispersion appear below ϵ_F unlike the Se-terminated cases. This makes the topological surface states better accessible and easily discernible

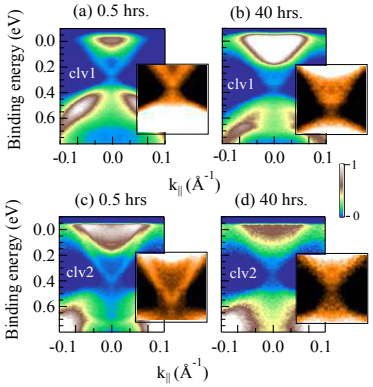

FIG. 4. Angle resolved photoemission (ARPES) data adapted from ref.[11]. ARPES data from Se-terminated surface (a) freshly cleaved and (b) 40 hours aged, and Bi-terminated surface (c) freshly cleaved and (d) 40 hours aged. Inset shows Dirac cone region with magnified intensity.

from the impurity bands.

In Fig. 3(e), we show the Fermi energy found in the slab calculations relative to that in the bulk calculation. While S1, S2 and S4 cases show an increase in Fermi energy, the Fermi energy becomes smaller than the bulk Fermi energy in S3 case. The S4 case (Bi terminated surface) exhibits the highest energy difference. Presence of 1 ML oxygen leads to a shift of the Fermi level towards higher energies suggesting an effective electron doping into the system for all the Se terminations. Ironically, the deposition of oxygen on Bi terminated surface (S4 case) leads to a shift of the Fermi level in opposite direction - towards lower energies suggesting an effective hole doping in this case consistent with the experimental observations [11].

It is clear that the electronic structure corresponding to different surface terminations of the system exhibit different scenario. The sample with Se1 bi-layer on top (S2 case) do not show Dirac cone although there are odd number of fermi level crossing of the energy bands between TRIMs. Here the top Se layers are weakly coupled with the bulk quintuple layer underneath and the surface electronic structure possess effectively two dimensional nature.

The samples with Se2, Se1 and Bi terminated surface as discussed in S1, S3 and S4 cases exhibit Dirac cone in their energy band structure. The presence of a layer of oxygen leads to instability of the Dirac states corresponding to the Se-terminated surface. In all the cases, the surface oxygen bands appear close to the Fermi level along with a shift of the Dirac cone to higher binding energies [11, 12]. Interestingly, the Bi-terminated surface exhibit more prominent Dirac states on oxygen deposited surface. In order to investigate the correspondence of this finding with the experimental scenario, we show the experimental angle resolved photoemission results in Fig. 4 adapted from the Ref.[11]. The experimental results

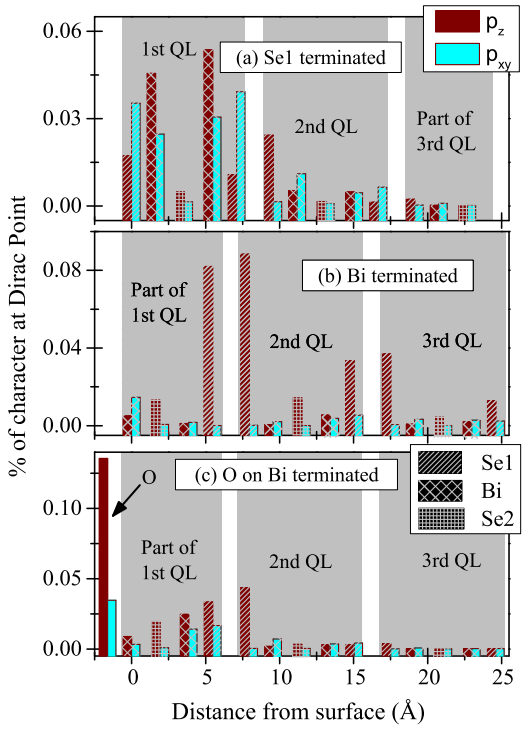

FIG. 5. Contribution to the Dirac point from different atomic layers. (a) S3, (b) S4 and (c) O on S4 terminations.

for the Se-terminated (Clv1) and Bi-terminated (Clv2) cases are shown in upper and lower panels of Fig. 4, respectively. The Freshly cleaved surface exhibit signature of Dirac cone in both the cases as expected. Oxygen accumulation on the Se-terminated surface leads to a shift of the Dirac point towards higher binding energy due to effective electron doping as found in this study too, along with a weakly defined Dirac cone. However, the Bi-terminated surface exhibits energy shift in opposite direction as predicted in Fig. 3(e) and exhibits a better defined conical shape of the Dirac cone. These results clearly corroborate the theoretical description shown in Fig. 3 establishing the robust nature of the Dirac states on Bi-terminated surface.

In order to understand the above scenario better, we investigate the character of the Dirac states in Fig. 5. The conduction band in this system consists of Se 4p and Bi 6p states. The Se 4p and Bi 6p contributions to the Dirac point (intensity within $\pm$50 meV across the Dirac point) obtained for different layers of Se1 terminated surface is shown in Fig. 5(a). The major contribution arises due to the hybridized states of Bi p and Se1 p states situated on both sides of the first quintuple layer [29]. Interestingly, the contribution from the interface of the first and second quintuple layers is most significant. The Dirac states consisting of Se1 (p_x,p_y) and Bi p_z states provide the largest contribution indicating their surface nature that is linked to the bulk via hybridization. In

addition, there is significant contribution from Se1 p_z-Bi (p_x, p_y) hybridized states. It is evident that the Dirac states in this system are not purely surface states, they are contributed by both surface and interface states involving top quintuple layer.

Ironically, the details of the Bi terminated case depicted in Fig. 5(b) exhibit an unusual scenario of Dirac states arising essentially from the interface states of first and second quintuple layers. This is different from the predicted surface behavior and demonstrate the complex nature of real materials. Here, the Se1 p_z states at the interface are strongly hybridized and form the Dirac states. In both the above cases, the Se layers at the interface of the successive quintuple layers appear to be quite strongly coupled. This explains why cleaving of these materials require strong force, thereby, employment of top-post removal method.

The presence of a layer of oxygen on Bi-terminated surface leads to significant change in the characteristics of the Dirac states. The Dirac states exhibit dominant surface character as shown in Fig. 5(c) along with significant reduction of the interface contributions. The large electronegativity of oxygen compared to all other constituent elements leads to an effective pulling of the electron cloud toward the surface. These results unambiguously demonstrate a way to engineer topological order on real systems, which can remain stable for long and can be used for various device application, realization of novel physics etc.

In summary, the density functional calculations of Bi_2Se_3 exhibit varied electronic structure on differently terminated surfaces. Although energy bands for every surface termination indicate cases of strong topological order, the signature of Dirac cone appears on Se1, Se2 and Bi terminated surfaces as defined by S1, S3 and S4 cases. We discover that the Dirac states are contributed by both sides of the top quintuple later with dominant contribution arising from the interface states rather than surface states of the pristine sample. Oxygenation leads to a shift of the Dirac point to higher binding energies for Se-terminated surface and makes the topological order weak. However, the Bi terminated surface is most robust and evolves to a better defined topological order. Robustness of topological surface states are the key factor for the technological applications of these materials and realization of various exotic physics such as Majorana Fermions, magnetic monopole etc. These results demonstrate ways of engineering Dirac states on real materials, which lays the all important building block in this field.

[1] M. Z. Hasan and C. L. Kane, Rev. Mod. Phys. **82**, 3045 (2010).
[2] L. Fu, C. L. Kane, and E. J. Mele, Phys. Rev. Letts. **98**, 106803 (2007).
[3] L. Fu and C. Kane, Phys. Rev. Letts. **100**, 096407 (2008).
[4] X.-L. Qi, R. Li, J. Zang, and S.-C. Zhang, Science **323**, 1184 (2009).
[5] D. Hsieh *et al.*, Nature **460**, 1101 (2009).
[6] H.-J. Noh *et al.*, Europhys. Letts. **81**, 57006 (2008).
[7] N. Fukui *et al.*, Phys. Rev. B **85**, 115426 (2012).
[8] M. Bianchi *et al.*, Nat. Commun. **1**, 128 (2010).
[9] X. Wang, G. Bian, T. Miller, and T.-C. Chiang, Phys. Rev. Letts. **108**, 096404 (2012).
[10] Z. Zhang and J. T. Yates Jr., Chem. Rev. **112**, 5520 (2012).
[11] D. Biswas, S. Thakur, K. Ali, G. Balakrishnan, and K. Maiti, *arXiv* 1411.0801v1.
[12] D. Kong *et al.*, ACS Nano **5**, 4698-4703 (2011).
[13] Y. L. Chen *et al.*, Science **329**, 659 (2010).
[14] L. V. Yashina *et al.*, ACS Nano **7**, 5181 (2013).
[15] V. V. Atuchin *et al.*, Crystal Growth & Design **11**, 5507 (2011).
[16] V. A. Golyashov *et al.*, J. Appl. Phys. **112**, 113702 (2012).
[17] P. Blaha, K. Schwarz, G. K. H. Madsen, D. Kvasnicka, and J. Luitz, WIEN2k An Augmented Plane Wave + Local Orbitals Program for Calculating Crystal Properties., K. Schwarz (ed.) (Techn. Universität Wien, Austria, 2001).
[18] M. I. Zargarova, P. K. Babaeva, D. S. Azhdarova, Z. D. Melikova, and S. A. Mekhtieva, Inorg. Mater. **31**, 263 (1995).
[19] K. Momma and F. Izumi, J. Appl. Crystallogr. **44**, 1272 (2011).
[20] Lin Hsin *et al.*, Nano Letts. **13**, 1915 (2013).
[21] J. P. Perdew, K. Burke, and M. Emzerhof, Phys. Rev. Letts. **77**, 3865 (1996).
[22] K. Maiti, Solid State Commun. **149**, 1351 (2009); R. S. Singh, V. R. R. Medicherla, K. Maiti, and E.V. Sampathkumaran, Phys. Rev. B **77** 201102(R), (2008).
[23] J. Black, E. M. Conwell, L. Seigle, and C. W. Spencer, J. Phys. Chem. Solids **2**, 240 - 251 (1957).
[24] E. Mooser and W. B. Pearson, Phys. Rev. **101**, 492 (1956).
[25] H. Zhang *et al.*, Nat. Phys. **5**, 438 (2009).
[26] K. Park, J. J. Heremans, V. W. Scarola, and D. Minic, Phys. Rev. Letts. **105**, 186801 (2010).
[27] K. Maiti, V. R. R. Medicherla, S. Patil, and R. S. Singh, Phys. Rev. Letts. **99**, 266401 (2007).
[28] K. Maiti, Europhys. Letts. **82**, 67006 (2008).
[29] Z.-H. Zhu *et al.*, Phys. Rev. Letts. **110**, 216401 (2013).